

The importance of ice sheet growth and retreat on magmatism and mantle CO₂ flux

John J. Armitage¹, David J. Ferguson², Kenni D. Petersen³, and Timothy T. Creyts⁴

¹Dynamique des Fluides Géologiques, Institut de Physique du Globe de Paris, Paris, France

²School of Earth and Environment, University of Leeds, Leeds, U.K.

³Department of Geoscience, University of Aarhus, Aarhus, Denmark

⁴Lamont-Doherty Earth Observatory, Columbia University, U.S.A

Key Points:

- We combine a new history of Icelandic ice-cover with a forward model of magma generation.
- Magmatism is influenced by both the rate of deglaciation and, importantly, the preceding growth of the ice sheet.
- For our model to be consistent with observations the rate of melt transport must be high.

16 **Abstract**

17 Climate cycles may significantly affect the eruptive behavior of terrestrial volcanoes due
 18 to pressure changes caused by glacial loading, which raises the possibility that climate
 19 change may modulate CO₂ degassing via volcanism. In Iceland, magmatism is likely to
 20 have been influenced by glacial activity. To explore if deglaciation therefore impacted
 21 CO₂ flux we coupled a model of glacial loading over the last ~120 ka to melt generation
 22 and transport. We find that a nuanced relationship exists between magmatism and glacial
 23 activity. Enhanced CO₂ degassing happened prior to the main phase of late-Pleistocene
 24 deglaciation, and it is sensitive to the duration of the growth of the ice sheet entering
 25 into the LGM, as well as the rate of ice loss. Ice sheet growth depresses melting in the
 26 upper mantle, creating a delayed pulse of CO₂ out-gassing as the magmatic system re-
 27 covers from the effects of loading.

28 **1 Introduction**

29 Evidence from several tectonic settings indicates that glaciated volcanic systems
 30 respond to changing ice volumes (Glazner, Manley, Marron, & Rojstaczer, 1999; Jellinek,
 31 Mange, & Saar, 2004; Jull & McKenzie, 1996; MacLennan, Jull, McKenzie, Slater, & Grönvöld,
 32 2002; Rawson et al., 2016; Sigvaldsson, Annertz, & Nilsson, 1992), and suggests there was
 33 a widespread volcanic response to late-Pleistocene ice retreat (Huybers & Langmuir, 2009).
 34 The most compelling evidence for climate-coupled volcanism comes from Iceland, where
 35 changes in early Holocene lava volumes and magma chemistry are consistent with de-
 36 pressurization during glacial unloading (Jull & McKenzie, 1996; MacLennan et al., 2002;
 37 Sinton, Grönvöld, & Saemundsson, 2005). Magma generation occurs due to pressure-release
 38 melting, as the mantle up-wells beneath rift zones. Although the net change in overbur-
 39 den pressures from variations in ice cover are relatively small, the high rates of change
 40 associated with glacial activity can produce significant short-term fluctuations in mag-
 41 matic output (Burley & Katz, 2015; Crowley, Katz, Huybers, Langmuir, & Park, 2015;
 42 Huybers & Langmuir, 2009; Lund & Asimow, 2011). Carbon readily partitions into mag-
 43 mas during partial melting (Rosenthal, Hauri, & Hirschmann, 2015) and is released as
 44 CO₂ gas at lower crustal pressures, making volcanism the primary pathway for trans-
 45 porting carbon from the Earth's mantle to the atmosphere (Dasgupta & Hirschmann,
 46 2010). Carbon is concentrated in early formed magma and does not enter the melt uni-
 47 formly over time. Therefore the extent to which glacially driven changes in primary magma
 48 generation alter the flux of CO₂ depends on where in the melting column melt produc-
 49 tion is enhanced, the rate of melt transport, and the history of ice sheet growth and re-
 50 treat.

51 Global data sets of the number of volcanic eruptions throughout the Pleistocene
 52 would suggest there is a correlation between climatic change and volcanism (Huybers
 53 & Langmuir, 2009), yet data resolution makes testing this association difficult. In Ice-
 54 land there are just over 300 published dated analysis of the Nb composition of Pleistocene
 55 lavas. This is arguably the most complete geochemical record within a region that ex-
 56 perienced significant Pleistocene deglaciation. In this study we take a new approach, and
 57 use a high resolution model of ice sheet history to drive a forward model of melt gen-
 58 eration and transport. We predict the change in eruption rates and melt composition
 59 as a function of the changing surface load, and also validate the predicted melt poros-
 60 ity against the seismic structure imaged below Iceland. We subsequently explore under
 61 what conditions climate and magmatism might be related, and the implications for CO₂
 62 degassing.

63 **2 Modelling of Melt Generation and Transport**

64 To investigate the impact of glacial activity on melt productivity, melt composi-
 65 tion, and CO₂ flux, we used a model of magma generation and transport coupled to a

flexural model for the response to change in load due to the ice sheet history (see Supplementary Material). The coupled model consists of a flexural model of the surface displacement due to the changing surface load as the ice sheet changes in thickness. This model of surface displacement is then coupled to either a 1D vertical column or a 2D corner flow model where the flow of the mantle is prescribed at either an upwelling rate of 10 or 20 mm yr⁻¹, or lateral spreading rate of 10 mm yr⁻¹. The higher upwelling rate incorporates the possible active effects of the Icelandic mantle plume (Kokfelt, Hoernle, & Hauff, 2003; MacLennan, McKenzie, & Gronvöld, 2001). The upwelling column is perturbed by the displacement due to loading, where the viscoelastic decay time of the load is set to 1000 yrs. Carbon partitioning into the melt is assumed to be governed by the coefficients derived by Rosenthal et al. (2015), and the mantle is assumed to be a depleted mix of primitive mantle and MORB. To approximate this depletion we assume a solidus-depletion gradient of 800 °C in line with melting experiments on depleted mantle (Wasylenki, Baker, Kent, & Stopler, 2003).

The surface expression of partial melting to glacial loading/unloading is influenced primarily by the rate at which the melt percolates through the mantle (Burley & Katz, 2015). To constrain the permeability of melt transport, we examined the effects of varying the permeability coefficient on the seismic properties of the mantle produced by our 1-D model. The thermal structure and porosity was converted to S-wave velocities, assuming that melt reduces the velocity by 7.9 % per percent porosity (Hammond & Humphreys, 2000) and including the effects of attenuation (Goes, Armitage, Harmon, Huismans, & Smith, 2012). Recent joint inversion of teleseismic and ambient noise Rayleigh waves in Iceland would suggest that the S-wave velocity is between 4 and 3.8 km s⁻¹ at depths of 50 to 150 km (Harmon & Rychert, 2016) (Figure 1). We find that the permeability coefficient needs to be relatively high (10^{-5} m²) giving a permeability, $k_\phi = k_0 \phi^3$, of the order of 10^{-14} m² ($\phi \approx 0.001$; Figure 1), because otherwise porosity would be too large and the S-wave velocity would decrease below the observed values. This permeability is an order of magnitude higher than the upper range used to explore how sea-level change might influence mid-ocean ridge (MOR) magmatism (Burley & Katz, 2015; Crowley et al., 2015), and suggests rates of magmatic ascent of the order of 10 m yr⁻¹. Previously it has been suggested that delays in signal propagation from the zone of partial melting at MORs to the surface might be of the order of a Milankovitch-scale period, 40 kyr (Huybers & Langmuir, 2017). However, the high permeability required to match the seismic observations from Iceland implies a magmatic system that much more rapidly responds to change in melting conditions, which is in agreement with the fast transport rates estimated from U-series isotope studies (Elliot & Spiegelman, 2014).

3 Glacial Forcing Throughout the Pleistocene

Iceland experienced extensive ice-cover during the last glacial period (Patton, Hubbard, Bradwell, & Schomackere, 2017), with maximum thicknesses in the center of the island of ~2km attained by ~23 ka (Figure 2a and b). Deglaciation after the LGM occurred at a varying rate, and was discontinuous. For example, a stage of re-advance occurred during the colder climate of the Younger Dryas (11.7-12.9 ka) (Nordahl & Ingólfsson, 2015). The final phase of deglaciation was particularly rapid, with the main volcanic zones being largely ice free by ~10 ka (Figure 2a). The most uncertain period of the glacial history is the pre-LGM growth of the ice sheet. To create the ice sheet histories shown in Figure 2b and Figure 3a we calibrated the ice volume since the LGM against the North Greenland Ice Core Project (NGRIP) δ¹⁸O record, and Quaternary sea-level curves assuming a linear correlation between these three signals (see Supplementary Material Text S1). We focus on two scenarios: M1, based on the ICE-5G sea-level curves (Peltier, 2004), and M2, based on the sea-level curves of Pico, Creveling, and Mitrovica (2017) (Figure S2).

We force our melt model with the 120 ka glacial history after a 5 Myr model wind-up to steady state (model M1, Figure 2b). The model predicts peaks in magmatic output and CO₂ flux as pressure changes due to loading and unloading impact the melt production rate (Figure 2). The response of the magmatic system to changes in ice cover varies depending on the mantle upwelling rate, the rate-of-change in ice sheet thickness, and the prior ice sheet history. Glacial loading suppresses melt production, leading to a decline in magma supply (see Supplementary Material, Figure S3). For example during the period between 35 and 15 ka, the growth of the ice sheet reduces eruption rates below 5 km of melt per Myr (Figure 2c). The recovery from this loading occurs initially in the deepest part of the system as this region is perturbed the least. Recovery is also faster if the mantle upwelling rate is higher, where an upwelling rate of 20 mm yr⁻¹ is more responsive than the equivalent 10 mm yr⁻¹ model (Figure 2b). Higher rates of change in surface loading will impact melt production more strongly such that small magnitude but rapid deglaciation events, for example at ~85 ka, have a relatively large effect on eruption rates (Figure 2c).

The impact of deglaciation events is modulated by the upwelling rate of the solid mantle because the upwelling rate controls the background productivity of the melting model. At slower upwelling rates, i.e. 10 mm yr⁻¹, some periods of deglaciation are not recorded in the flux of magma erupted. An example of this is the warming event at 60 ka (Figure 2), where the 10 mm yr⁻¹ upwelling model produces no response in either the eruption rate or CO₂ flux. If however upwelling is more rapid, 20 mm yr⁻¹, then there is a clear pulse in melt eruption rate (Figure 2). This is because porosity and productivity are so low, that any pulse in melt production does not reach the surface.

Our models indicate that deglaciation-enhanced melt productivity is not only a function of the rate of deglaciation, but is strongly dependent on the preceding glacial history. For example, in the 20 mm yr⁻¹ upwelling rate model, the largest CO₂ peak is estimated to occur at ~60 ka and not during the volumetrically larger magmatic pulse at the end of the Pleistocene (Figure 2d). This difference is because when the ~60 ka warming occurred, the melt was enriched in carbon due to the preceding rapid glaciation. Magmas erupted during the Late-Pleistocene pulse were more depleted in carbon compared to those in the 60 ka event.

4 Glacial Forcing Through the Latest Pleistocene and Holocene

There are two distinct late Pleistocene magmatic pulses, separated by the Younger Dryas cold period (Figure 3a and b). However, for the model M2 ice sheet history there are three pulses in CO₂ flux at the end of the Pleistocene, due to the faster ice sheet growth entering the LGM from 35 to 25 ka in this model (Figure 3a and e). This peak in CO₂ flux is because the small magnitude but rapid deglaciations after 25 ka tap melts rich in trace elements including Nb and carbon (Figure 3c and d).

The observed time series of incompatible trace element concentrations in Icelandic magmas and ice sheet history have been suggested to be strongly associated (Eason, Sinton, Gronvöld, & Kurz, 2015; Gee, Taylor, Thirwall, & Murton, 1998; Jull & McKenzie, 1996; MacLennan et al., 2002; Sinton et al., 2005). We find that the predicted change in Nb, which behaves in a similar way to C during mantle melting (Rosenthal et al., 2015), from all our models fit within the range of the observations (Figure 3c). The M2 model gives the strongest signature in Nb concentrations of deglaciation during the end of the Pleistocene, while the signature is more subdued in the M1 ice sheet model (Figure 3c). The 1D forward model used is highly idealised, and yet the agreement between the observations and model is encouraging, and suggests the compositional change observed in lavas erupted during the late-Pleistocene to early Holocene is due to rapid deglaciation (Eason et al., 2015; Gee et al., 1998; MacLennan et al., 2002; Sinton et al., 2005). This implies that the observed change in melt composition is due to change in ice sheet

168 loading and that the pre-deglaciation volcanism likely released a significant volume of
 169 CO₂ (Figure 3e).

170 The 1D column model will underestimate the impact of change in deep melt pro-
 171 ductivity, as it cannot capture the deep wings of the zone of partial melting. To explore
 172 the impact of this we force a series of 1D models with the vertical flow taken from steady
 173 state corner flow perturbed by the flexural response of the deglaciation of a 200 km wide
 174 ice sheet. The half spreading rate is assumed to be 10 mm yr⁻¹, and the mantle poten-
 175 tial temperature is 1450 °C. Melt travels vertically from the zone of partial melting in
 176 columns at 0 to 80 km from the rift axis (Figure 4). We find that in the central zone, from
 177 the ridge centre to 40 km distance, the trend in Nb and CO₂ flux is relatively similar,
 178 with a reduction in Nb at 15 ka. At distances greater than 40 km, a peak in Nb and CO₂
 179 flux is predicted to occur with an increasing delay compared to the centre of extension
 180 (Figure 4).

181 The full solution to the coupled equations of magma dynamics would suggest that
 182 melts generated at a distance of up to 60 km from the centre of extension are advected
 183 to the ridge axis (Katz, 2008). If all of the melt generated up to 60 km from the centre
 184 of extension is erupted, then the CO₂ flux is significantly increased during the Holocene
 185 due to the addition input of melt from the distal parts of the zone of partial melting (Fig-
 186 ure 4b). Therefore these low productivity and deep regions of the zone of partial melt-
 187 ing might be a key exporter of mantle carbon into the atmosphere. However, the range
 188 of observed Nb concentrations are relatively similar to the axial concentrations, from within
 189 <40 km of the rift centre (Figure 4). This would suggest that the widest regions of the
 190 zone of partial melting are not sampled by the volcanism in the Reykjanes Ridge and
 191 Western Volcanic Zone, leading to an estimate of CO₂ fluxes more in line with the sim-
 192 pler 1D model.

193 5 Discussion and Conclusions

194 The models imply that the deglaciation beginning at 18 ka and continuing through
 195 the Bolling warming at 14.8 ka released substantial quantities of CO₂ when compared
 196 to the last 120 ka (Figure 3c and Figure 4b), and this elevated CO₂ release was because
 197 of the preceding growth of the ice sheet. Volcanism during this time would have taken
 198 place in a sub-glacial environment and unsurprisingly does not feature in the post-glacial
 199 sub-aerial record. Evidence from sub-glacial volcanic units (tuyas) erupted during this
 200 time period (Hartley, Thordarson, & de Joux, 2016) suggest volumetric and composi-
 201 tional trends consistent with those predicted by our model (Figure 3c and Figure 4).

202 Forcing our model with the long-term 120 ka ice sheet history produces a periodic
 203 fluxing of CO₂ from Icelandic volcanoes due to ice-loss events over this period, implying
 204 a close link between ice dynamics and magmatic out-gassing. The greatest release
 205 of CO₂, however, occurred during the period of ice-loss just before the Younger Dryas
 206 (~14 ka), and therefore before the largest phase of late-Pleistocene deglaciation (Figure
 207 4). The concentration of CO₂ released in this magmatic pulse was enhanced due to the
 208 lack of any significant loss of ice volume since ~40 ka. This created a magmatic system
 209 capable of fluxing large volumes of carbon during the initial period of post-LGM deglaci-
 210 ation (both models M1 and M2, Figure 3e), and such a pulse of atmospheric CO₂ is thought
 211 to be recorded at between 15 and 14 ka in the EPICA Dome C ice core (Köhler, Knorr,
 212 Buiron, Lourantou, & Chappellaz, 2011). It is therefore possible that this pulse of CO₂
 213 bolstered the climate warming, and final phase of deglaciation, that proceeded the Younger
 214 Dryas.

215 The CO₂ flux due to deglaciation is strongly influenced by the prior ice sheet growth.
 216 It is the sustained growth of the Icelandic ice sheet before 25 ka lead to the significant
 217 pulse in volcanism and CO₂ upon deglaciation at the end of the Pleistocene (Figure 4).

This would imply that while a rapid loss of mass can trigger increased eruptions, the impact on atmospheric CO₂ concentrations is strongly modulated by the full history of the changing surface load. In effect we cannot conclude that all deglaciation events, or other rapid unloading events due to for example erosion, lead to a large flux of volatile gases into the Earth's atmosphere. The Earth system is more complex than such simple causality, yet one clear implication is that deglaciation after a prolonged period of ice-house conditions will lead to a significant carbon degassing of the upper mantle.

Supporting Information

A detailed discussion of the methodology can be found in the supporting information (Andersen et al., 2004; Andrews, 2008; Armitage, Collier, Minshull, & Henstock, 2011; Clark et al., 2009; Geirsdóttir, 2011; Gibson & Geist, 2010; Gureenko & Chaussidon, 1995; Katz, Spiegelman, & Langmuir, 2003; Lambeck & Chappel, 2001; Lambeck, Rouby, Purcell, Sun, & Sambridge, 2014; McKenzie & O'Nions, 1991; Miller, Zhu, Montési, & Gaetani, 2014; Ribe, 1985; Scott, 1992; Shortle & MacLennan, 2011; Silbeck, 1975; Sleep & Snell, 1976; Spiegelman, 1996; Spratt & Lisicki, 2016).

Acknowledgments

We would like to thank M. A. Mary Gee (The University of Western Australia) for sharing her Nb composition data from the Reykjanes Peninsular, and Tamara Pico (Harvard University) for sharing her sea level curves. John J. Armitage acknowledges funding from an Agence National de la Recherche (France), Accueil de Chercheurs de Haute Niveau, grant InterRift. The 1-D melting model is available from <https://bitbucket.com/johnjarmitage/melt1d-icesheet/>

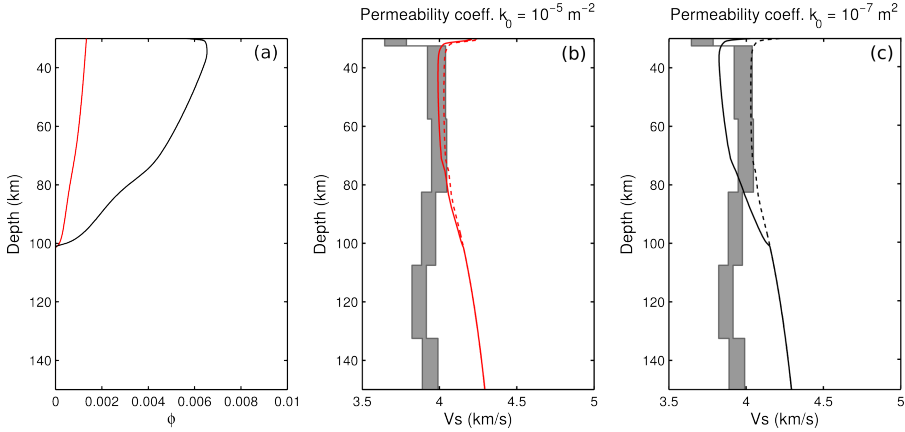
References

- Andersen, K. K., Azuma, N., Barnola, J. M., Bigler, M., Biscaye, P., Caillon, N., ... White, J. W. C. (2004). High-resolution record of northern hemisphere climate extending into the last interglacial period. *Nature*, *431*, 174-151. (doi: 10.1038/nature02805)
- Andrews, J. T. (2008). The role of the Iceland Ice Sheet in the North Atlantic during the late Quaternary: a review and evidence from Denmark Strait. *Journal of Quaternary Science*, *23*, 3-20. (doi: 10.1002/jqs.1142)
- Armitage, J. J., Collier, J. S., Minshull, T. A., & Henstock, T. J. (2011). Thin oceanic crust and flood basalts: India-Seychelles breakup. *Geochemistry Geophysics Geosystems*, *12*(Q0AB07). (doi:10.1029/2010GC003316)
- Burley, J. M. A., & Katz, R. F. (2015). Variations in mid-ocean ridge CO₂ emissions driven by glacial cycles. *Earth and Planetary Science Letters*, *426*, 246-258. (doi: 10.1016/j.epsl.2015.06.031)
- Clark, P. U., Dyle, A. S., Shakun, J. D., Carlson, A. E., Clark, J., Wohlfarth, B., ... McCabe, A. M. (2009). The last glacial maximum. *Science*, *325*, 710. (doi: 10.1126/science.1172873)
- Crowley, J. W., Katz, R. F., Huybers, P., Langmuir, C. H., & Park, S. H. (2015). Glacial cycles drive variations in the production of oceanic crust. *Science*, *347*, 1237-1240. (doi: 10.1126/science.1261508)
- Dasgupta, R., & Hirschmann, M. M. (2010). The deep carbon cycle and melting in Earth's interior. *Earth and Planetary Science Letters*, *298*, 1-13. (doi: 10.1016/j.epsl.2010.06.039)
- Eason, D. E., Sinton, J. M., Gronvöld, K., & Kurz, M. D. (2015). Effects of deglaciation on the petrology and eruptive history of the Western Volcanic Zone, Iceland. *Bulletin of Volcanology*, *77*(47). (doi: 10.1007/s00445-015-0916-0)

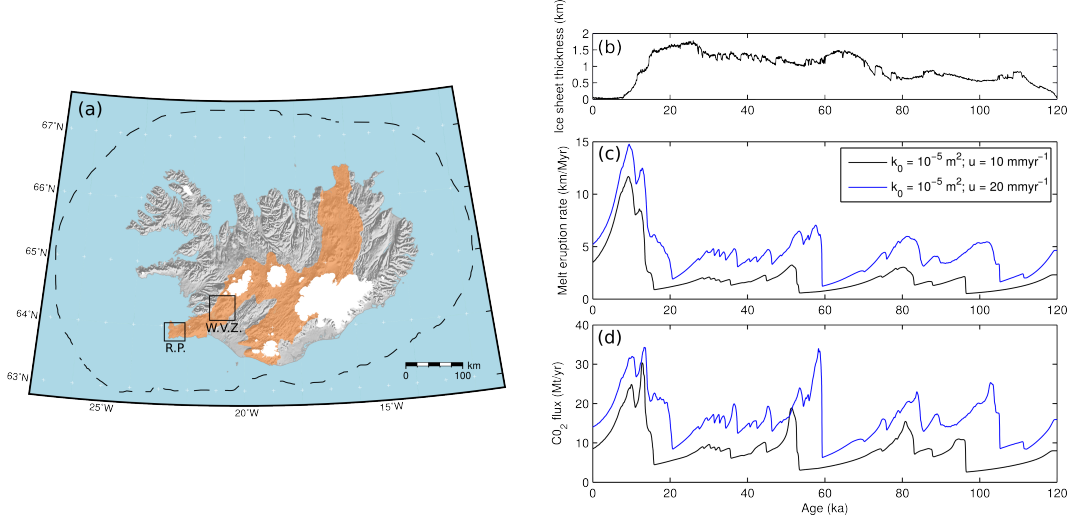
- 267 Elliot, T., & Spiegelman, M. (2014). Melt migration in oceanic crustal production:
 268 A u-series perspective. In *Treatise on geochemistry* (2nd ed., p. 543-581). Else-
 269 vier. (doi: 10.1016/B978-0-08-095975-7.00317-X)
- 270 Gee, M. A. M., Taylor, R. N., Thirwall, M., & Murton, B. J. (1998). Glacioisostacy
 271 controls chemical and isotopic characteristics of tholeiites from the Reykjanes
 272 Peninsula, SW Iceland. *Earth and Planetary Science Letters*, 164, 1-5.
- 273 Geirsdóttir, A. (2011). Pliocene and pleistocene glaciations of iceland: a brief
 274 overview of the glacial history. In J. Ehlers, P. L. Gibbard, & P. Hughes
 275 (Eds.), *Quaternary glaciations - extent and chronology, a closer look* (Vol. 15,
 276 p. 199-210). Elsevier. (doi: 10.1016/B978-0-444-53447-7.00016-7)
- 277 Gibson, S. A., & Geist, D. (2010). Geochemical and geophysical estimates of litho-
 278 spheric thickness variation beneath galápagos. *Earth and Planetary Science
 279 Letters*, 300, 275-286. (doi: 10.1016/j.epsl.2010.10.002)
- 280 Glazner, A. F., Manley, C. R., Marron, J. S., & Rojstaczer, S. (1999). Fire
 281 or ice: Anticorrelation of volcanism and glaciation in california over the
 282 past 800,000 years. *Geophysical Resaerch Letters*, 26, 1759-1762. (doi:
 283 10.1029/1999GL900333)
- 284 Goes, S., Armitage, J. J., Harmon, N., Huismans, R., & Smith, H. (2012). Low seis-
 285 mic velocities below mid-ocean ridges: Attenuation vs. melt retention. *Journal
 286 of Geophysical Research*, 117, B12403. (doi: 10.1029/2012JB009637)
- 287 Gurenko, A. A., & Chaussidon, M. (1995). Enriched and depleted primitive melts
 288 included in olivine from icelandic tholeiites: Origin by continuous melting of a
 289 single mantle column. *Geochimica et Cosmochimica Acta*, 59, 2905-2917.
- 290 Hammond, W. C., & Humphreys, E. D. (2000). Upper mantle seismic wave ve-
 291 locity: Effects of realistic partial melt geometries. *Journal of Geophysical Re-
 292 search*, 105, 10975-10986.
- 293 Harmon, N., & Rychert, C. A. (2016). Joint inversion of teleseismic and ambient
 294 noise Rayleigh waves for phase velocity maps, an application to Iceland. *Jour-
 295 nal of Geophysical Research*, 121, 5966-5987. (doi: 10.1002/2016JB012934)
- 296 Hartley, M. E., Thordarson, T., & de Joux, A. (2016). Postglacial eruptive history
 297 of the Askja region, North Iceland. *Bulleting of Volcanology*, 78(28). (doi:
 298 10.1007/s00445-016-1022-7)
- 299 Huybers, P., & Langmuir, C. H. (2009). Feedback between deglacation, volca-
 300 nism, and atmospheric CO₂. *Earth and Planetary Science Letters*, 286, 479-491.
 301 (doi: 10.1016/j.epsl.2009.07.014)
- 302 Huybers, P., & Langmuir, C. H. (2017). Delayed CO₂ emissions from mid-ocean
 303 ridge volcanism as a possible cause of late-Pleistocene glacial cycles. *Earth and
 304 Planetary Science Letters*, 457, 238-249. (doi: 10.1016/j.epsl.2016.09.021)
- 305 Jellinek, M. A., Mange, M., & Saar, M. O. (2004). Did melting glaciers
 306 cause volcanic eruptions in eastern california? probing the mechanisms
 307 of dike formation. *Journal of Geophysical Research*, 109(B09206). (doi:
 308 10.1029/2004JB002978)
- 309 Jull, M., & McKenzie, D. (1996). The effect of deglaciation on mantle melting be-
 310 neath Iceland. *Journal of Geophysical Research*, 101(B10), 21815-21828.
- 311 Katz, R. F. (2008). Magma dynamics with the enthalpy method: Benchmark so-
 312 lutions and magmatic focusing at mid-ocean ridges. *Journal of Petrology*, 49,
 313 2099-2121. (doi:10.1093/petrology/egn058)
- 314 Katz, R. F., Spiegelman, M., & Langmuir, C. H. (2003). A new parameterization of
 315 hydrous mantle melting. *Geochemistry Geophysics Geosystems*, 4, 1073. (doi:
 316 10.1029/2002GC000433)
- 317 Köhler, P., Knorr, G., Buiron, D., Lourantou, A., & Chappellaz, J. (2011). Abrupt
 318 rise in atmospheric CO₂ at the onset of the Bolling/Allerod: in-situ ice core
 319 data versus true atmospheric signals. *Climate of the Past*, 7, 473-486. (doi:
 320 10.5194/cp-7-473-2011)
- 321 Kokfelt, T. F., Hoernle, K., & Hauff, F. (2003). Upwelling and melting of the Ice-

- 322 land plume from radial variation of ^{238}U - ^{230}Th disequilibria in postglacial
 323 volcanic rocks. *Earth and Planetary Science Letters*, 214, 176-186. (doi:
 324 10.1016/S0012-821X(03)00306-6)
- 325 Lambeck, K., & Chappel, J. (2001). Sea level change through the last glacial cycles.
 326 *Science*, 292, 679-686. (doi: 10.1126/science.1059549)
- 327 Lambeck, K., Rouby, H., Purcell, A., Sun, Y., & Sambridge, M. (2014). Sea level
 328 and global ice volumes from the Last Glacial Maximum to the Holocene.
 329 *Proceedings of the National Academy of Sciences*, 111, 15296-15303. (doi:
 330 10.1073/pnas.141176211)
- 331 Lund, D. C., & Asimow, P. D. (2011). Does sea level influence mid-ocean ridge mag-
 332 matism on Milankovitch timescales? *Geochemistry Geophysics Geosystems*,
 333 12(Q12009). (doi: 10.1029/2011GC003693)
- 334 MacLennan, J., Jull, M., McKenzie, D., Slater, L., & Gronvöld, K. (2002). The
 335 link between volcanism and deglaciation in Iceland. *Geochemistry Geophysics
 336 Geosystems*, 3(11, 1062). (doi: 10.1029/2001GC000282)
- 337 MacLennan, J., McKenzie, D., & Gronvöld, K. (2001). Plume-driven upwelling un-
 338 der central Iceland. *Earth and Planetary Science Letters*, 194, 67-82. (doi:
 339 10.1016/S0012-821X(01)00553-2)
- 340 McKenzie, D., & O'Nions, R. K. (1991). Partial melt distribution from inversion of
 341 rare earth element concentrations. *Journal of Petrology*, 32, 1021-1091.
- 342 Miller, K. J., Zhu, W., Montési, L. G. J., & Gaetani, G. A. (2014). Experimental
 343 quantification of permeability of partially molten mantle rock. *Earth and Plan-
 344 etary Science Letters*, 388, 273-282. (doi: 10.1016/j.epsl.2013.12.003)
- 345 Nordahl, H., & Ingólfsson, O. (2015). Collapse of the Icelandic ice sheet controlled
 346 by sea level rise? *Arktos*, 1, 1-13. (doi: 10.1007/s41063-015-0020-x)
- 347 Patton, H., Hubbard, A., Bradwell, T., & Schomackere, A. (2017). The configura-
 348 tion, sensitivity and rapid retreat of the Late Weichselian Icelandic ice sheet.
 349 *Earth-Science Reviews*, 166, 223-245. (doi: 10.1016/j.earscirev.2017.02.001)
- 350 Peltier, W. R. (2004). Global glacial isostacy and the surface of the ice-age Earth:
 351 The ICE-5G (VM2) model and grace. *Annual Reviews of Earth and Planetary
 352 Science*, 32, 111-149. (2004)
- 353 Pico, T., Creveling, J. R., & Mitrovica, J. X. (2017). Sea-level records from the
 354 U.S. mid-Atlantic constrain Laurentide Ice Sheet extent during Marine Isotope
 355 Stage 3. *Nature Communications*, 8(15621). (doi: 10.1038/ncomms15612)
- 356 Rawson, H., Pyle, D. M., Mather, T. A., Smith, V. S., Fontjin, K., Lachowycz,
 357 S. M., & Naranjo, J. A. (2016). The magmatic and eruptive response of arc
 358 volcanoes to deglaciation: Insights from southern Chile. *Geology*, 44, 251-254.
 359 (doi: 10.1130/G37504.1)
- 360 Ribe, N. M. (1985). The generation and composition of partial melts in the earth's
 361 mantle. *Earth and Planetary Science Letters*, 73, 361-376.
- 362 Rosenthal, A., Hauri, E. H., & Hirschmann, M. M. (2015). Experimental determi-
 363 nation of C, F, and H partitioning between mantle minerals and carbonated
 364 basalt, CO₂/Ba and CO₂/Nb systematics of partial melting, and the CO₂
 365 contents of basaltic source regions. *Earth and Planetary Science Letters*, 415,
 366 77-87. (doi: 10.1016/j.epsl.2014.11.044)
- 367 Scott, D. R. (1992). Small-scale convection and mantle melting beneath mid-ocean
 368 ridges. In J. Phipps Morgan, D. K. Blackman, & J. M. Sinton (Eds.), *Mantle
 369 flow and melt generation at mid-ocean ridges* (Vol. Geophysical Monograph 71,
 370 p. 327-352). American Geophysical Union.
- 371 Shorttle, O., & MacLennan, J. (2011). Compositional trends of icelandic
 372 basalts: Implications for short-length scale lithological heterogeneity in
 373 mantle plumes. *Geochemistry Geophysics Geosystems*, 12, Q11008. (doi:
 374 10.1029/2011GC003748)
- 375 Sigvaldsson, G. E., Annertz, K., & Nilsson, M. (1992). Effect of glacier load-
 376 ing/delowering on volcanism: postglacial volcanic production rate of the Dyn-

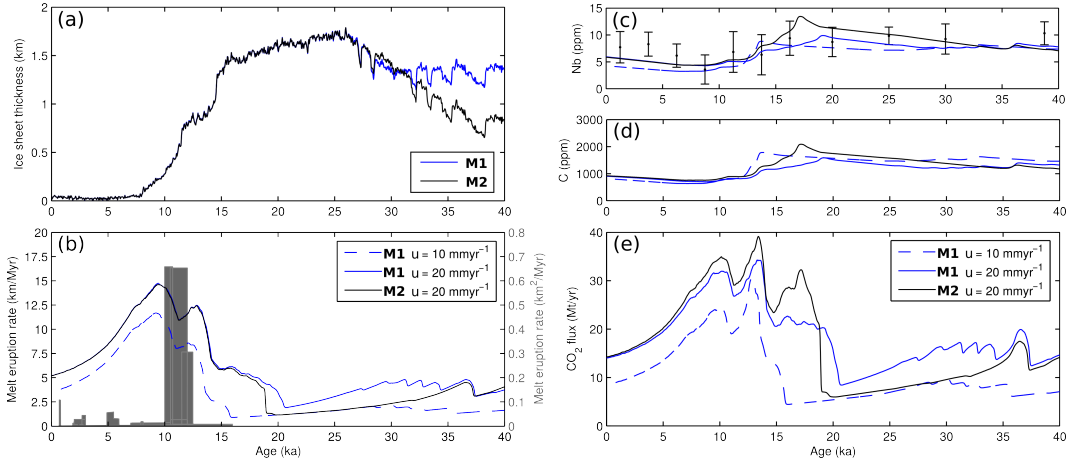
- 377 gjufjöll area, central Iceland. *Bulletin of Volcanology*, 54, 385-392. (doi:
378 10.1007/BF00312320)
- 379 Silbeck, J. N. (1975). On the fluid dynamics of ridge crests. In *Notes on the 1975*
380 *summer study program in geophysical fluid dynamics at the Woods Hole Oceanographic*
381 *Institution*, (Vol. 2, p. 113-122).
- 382 Sinton, J., Grönvold, K., & Saemundsson, K. (2005). Postglacial eruptive history
383 of the Western Volcanic Zone, Iceland. *Geochemistry Geophysics Geosystems*,
384 6(Q12006). (doi: 10.1029/2005GC001021)
- 385 Sleep, N. H., & Snell, N. S. (1976). Thermal contraction and flexure of mid-
386 continent and Atlantic marginal basins. *Geophysical Journal of the Royal*
387 *Astronomical Society*, 45, 125-154.
- 388 Spiegelman, M. (1996). Geochemical consequences of melt transport in 2-D: The
389 sensitivity of trace elements to mantle dynamics. *Earth and Planetary Science*
390 *Letters*, 139, 115-132.
- 391 Spratt, R. M., & Lisiecki, L. E. (2016). A late Pleistocene sea level stack. *Climate of*
392 *the Past*, 12, 1079-1092. (doi: 10.5194/cp-12-1079-2016)
- 393 Wasylewski, L. E., Baker, M. B., Kent, A. J. R., & Stopler, E. M. (2003). Near-
394 solidus melting of the shallow upper mantle: partial melting experiments on
395 depleted peridotite. *Journal of Petrology*, 44, 116-1191.



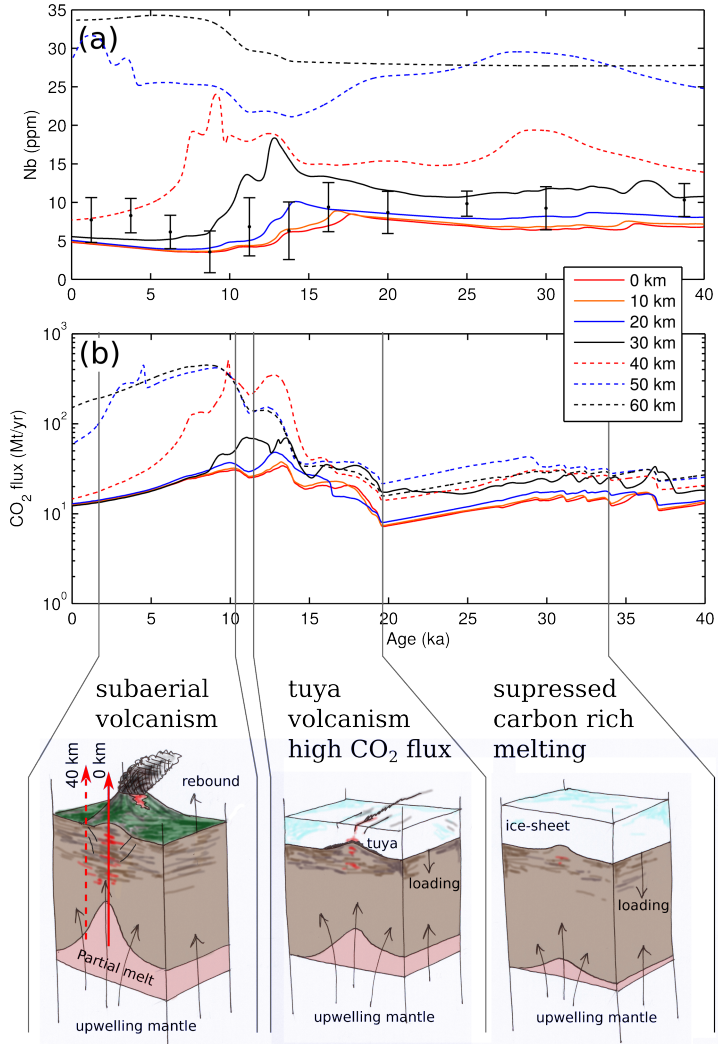
396 **Figure 1.** Profiles of porosity and S-wave seismic velocity for the two model permeabilities of
 397 $k_0 = 10^{-7} \text{ m}^2$ black line, and $k_0 = 10^{-5} \text{ m}^2$ red line. (a) Porosity plotted against depth at steady
 398 state. (b) S-wave velocity from the joint inversion of teleseismic and ambient noise Rayleigh
 399 waves (Harmon & Rychert, 2016) and the predicted S-wave profile from the high permeability
 400 case. The model includes the addition of the adiabatic gradient, the anharmonic effects from the
 401 mineralogy and effects of attenuation (Goes et al., 2012). The dashed line assumes melt has no
 402 effect, the solid line includes a 7.9 % reduction in V_S per percent melt (Hammond & Humphreys,
 403 2000). (c) S-wave velocity predictions for the low permeability case.



404 **Figure 2.** Response of the model to periodic and observed ice sheet thickness changes of the
 405 last 120 ka. (a) Map of Iceland showing the locations of the volcanic rift zones in orange and the
 406 maximum extent of the ice sheet at the last glacial maximum (dashed line). The boxes show the
 407 location of the Reykjanes Peninsular (R. P.) and the Western Volcanic Zone (W. V. Z.). (b) The
 408 ice sheet thickness predicted from the ice sheet model M1 over the last 120 ka. (c) Melt eruption
 409 rate and (d) carbon flux response to the step change in ice sheet thickness: black line, an upper
 410 mantle permeability coefficient of $k_0 = 10^{-5} \text{ m}^2$ and upwelling velocity of 10 mm yr^{-1} , and blue
 411 line, an upwelling velocity of 20 mm yr^{-1} .



412 **Figure 3.** Impact of ice sheet growth and decay on melt eruption and composition over the
 413 last 40 ka. (a) Ice sheet models M1 and M2 taken from the sea-level models of Peltier (2004) and
 414 Pico et al. (2017) respectively. (b) Melt eruption rates (in km of melt per Myr): blue solid line,
 415 ice sheet history 5G for $k_0 = 10^{-5} \text{ m}^2$ with an upwelling rate of 20 mm yr^{-1} ; blue dashed line, M1
 416 for $k_0 = 10^{-5} \text{ m}^2$ with an upwelling rate of 10 mm yr^{-1} ; black solid line, ice sheet history M2 for
 417 $k_0 = 10^{-5} \text{ m}^2$ with an upwelling rate of 20 mm yr^{-1} . The gray region shows estimated eruption
 418 rates from geological observations (5) (in km^2 of melt per Myr). (c) Observed and predicted Nb
 419 concentrations (ppm), observations are from the Reykjanes Peninsula and the Western Volcanic
 420 Zone (Eason et al., 2015; Gee et al., 1998; Sinton et al., 2005) and are binned at 2.5 kyr intervals
 421 from 0 to 17.5 ka and then at 5 kyr intervals. (d) Predicted variation of in the concentration of
 422 carbon (ppm) within the erupted melt. (e) Predicted variation in the flux of CO₂, assuming that
 423 the flux of CO₂ that Icelandic volcanism covers an area of $30,000 \text{ km}^2$, and CO₂ (ppm) = 3.67 C
 424 (ppm) (see Eq. 23 in the Supplementary Material).



425 **Figure 4.** Impact of glacial history on off-axis and on-axis melting. A series of 1D column
 426 melting models forced by the response to deglaciation (ice sheet history model M1) where the
 427 mantle flow is of steady state corner flow. (a) Nb concentrations from the centre of extension out
 428 to 60 km from the centre of extension. The mean concentration weighted by the eruption rate is
 429 plotted as the thick black line. (b) Predicted CO₂ flux from the series of vertical melting models.
 430 The late-Pleistocene eruptions are typified by tuya magmatism. This will have been the case up
 431 until at least ~14 ka, where either magmatism was suppressed or when eruptions occurred they
 432 will have been beneath at least 1 km of ice-cover (Hartley et al., 2016). The suppressed melting
 433 regime will have become carbon rich because the shallow low-C melt production is damped due
 434 to the ice-sheet loading. Upon deglaciation there is increased volcanism, which initially taps the
 435 melt rich carbon.